Paper published as: Prudhomme, M., Lakhdar, C., Fattaccioli, J., Addouche, M., Chollet, F., Functionalization of microbubbles in a microfluidic chip for biosensing application. Biomed Microdevices 26, 39 (2024). https://doi.org/10.1007/s10544-024-00721-2

Functionalization of microbubbles in a microfluidic chip for biosensing application

Marc Prudhomme[1], Chaimaa Lakhdar[1], Jacques Fattaccioli[2,3], Mahmoud Addouche[1], Franck Chollet[1*]

[1]Institut FEMTO-ST, Université de Franche-Comté, CNRS, Besançon, F-25000 France.
[2]PASTEUR, Département de Chimie, Ecole Normale Supérieure, PSL Université, Sorbonne Université, CNRS, F-75005, Paris, France.
[3]Institut Pierre-Gilles de Gennes pour la Microfluidique, F-75005, Paris, France.

*Corresponding author(s). E-mail(s): franck.chollet@femto-st.fr;

Abstract

Microbubbles are widely used for biomedical applications, ranging from imagery to therapy. In these applications, microbubbles can be functionalized to allow targeted drug delivery or imaging of the human body. However, functionalization of the microbubbles is quite difficult, due to the unstable nature of the gas/liquid interface. In this paper, we describe a simple protocol for rapid functionalization of microbubbles and show how to use them inside a microfluidic chip to develop a novel type of biosensor. The microbubbles are functionalized with biochemical ligand directly at their generation inside the microfluidic chip using a DSPE-PEG-Biotin phospholipid. The microbubbles are then organized inside a chamber before injecting the fluid with the bioanalyte of interest through the static bubbles network. In this proof-of-concept demonstration, we use streptavidin as the bioanalyte of interest. Both functionalization and capture are assessed using fluorescent microscopy thanks to fluorescent labeled chemicals. The main advantages of the proposed technique compared to classical ligand based biosensor using solid surface is its ability to rapidly regenerate the functionalized surface, with the complete functionalization/capture/measurement cycle taking less than 10 min.

Keywords: microbubble, surface functionalization, biosensor, reusable

1 Introduction

Gas microbubbles (MBs) are used in many applications, due to their particular acoustic response. One of the first and now most common application is in ultrasound medical imagery. Gramiak and Shah (1968) found out by accident that the bubbles formed by cavitation in a saline solution injected for the echocardiography of the aortic root scattered effectively the ultrasounds. Since then, microbubbles are used as Ultrasound Contrast Agents (UCAs) to enhance the acoustic response of the human blood pool (Versluis et al. (2020)). Once injected in the vasculature, the non linear acoustic response of the microbubbles produce an acoustic radiation over a range of frequencies that distinguish the vessels from the surrounding tissue, allowing its visualisation. In order to increase the stability of the microbubbles used for imaging, they are coated with a biocompatible shell, that can be made of lipid, polymer, sugar or protein material (Kogan et al. (2010)). The shell allows to decreases the interfacial tension and the corresponding capillary pressure which stabilizes the bubble by avoiding its dissolution, and also form a barrier against gas diffusion. Based on the research related to UCAs, microbubbles have been used more recently for therapy and drug delivery as Ultrasound Triggered Agents (UTAs) (Unger et al. (2002)). Incorporating drugs with microbubbles and release it on demand using ultrasound allow to reduce toxic side effect while increasing the precision of the treatment. There are different ways to transport drugs or genes thanks to microbubbles and this technique is more efficient with highly active drugs that do not require large quantities. The most known therapeutic technique involving oscillating microbubbles is called sonoporation, where high intensity ultrasound combined with microbubbles can efficiently and temporarily increase the cell membrane permeability, leading to the creation of pores that facilitate the incorporation of drugs (Chowdhury et al. (2020)). Nowadays, this technique is used especially in cancer therapy or cardiovascular diseases, among others (Unger et al. (2002); Chowdhury et al. (2020); Unger et al. (2014)). In order to perform targeted imaging or to increase the accuracy of drugs delivery, the microbubbles can be decorated at their surface with biochemical ligands able to adhere to a specific region of interest on the targeted biological analyte. Microbubbles are traditionally decorated with antibodies or small peptides, but recent developments (Langeveld et al. (2021)) report novel strategies for developing targeting microbubbles (tMB) both for imaging and therapy applications. Current trends are in the development of magnetic responsive microbubbles thanks to the incorporation of lipid coated magnetic nanoparticles at MBs surface (Beguin et al. (2019)), multiple targets tMB with the incorporation of two or more ligands at the microbubbles surface (Warram et al. (2011)), and in development of new ligands on tMB allowing novel applications in imaging and therapy, such as detection of specific diseases (Yang et al. (2021)). For the latter, the new ligand is coupled to the tMB surface using a streptavidin-biotin bridge. The non covalent bond between biotin and streptavidin is one of the strongest interaction in nature, but, its clinical use is limited as streptavidin presents some immunogenicity issue (Dundas et al. (2013)).

In this paper, we try to develop a novel application for functionalized MBs by using them for bio-sensing (Fig. 1). More precisely, we aim to use their ability to self organize in dense array and use their surface as functionalized biointerface for the capture

of biological analytes. After capture, the detection/quantification of the bioanalytes may simply be obtained with fluorescence if the analyte is fluorescent or labeled but it may even rely on label free detection by probing the mechanical properties of the MBs surface. In any case, by using the surface of MBs, we may largely improve the operation of classical biosensors using microfluidic detection chambers (Squires et al. (2008), Oseev et al. (2021)). Actually we will avoid planar solid biointerfaces, slow to decorate with ligand and hard to regenerate, while we may have a better capture efficiency for the bioanalyte of interest (Azzopardi et al. (2019)). We will present here all the fluidic aspects of the development and operation of the sensor, especially the fast on-chip functionalization of the MBs surface and the capture of a bionalyte. In this seminal work, the detection method is based on fluorescent imaging. In order to demonstrate the technology, we will use the couple biotin-streptavidin, where the biotin will be the ligand that will decorate the MBs surface for capturing green labeled streptavidin, the analyte of interest. We note that the immunogenicity of the couple is not a problem in this application, as the sensor is working outside of the human body.

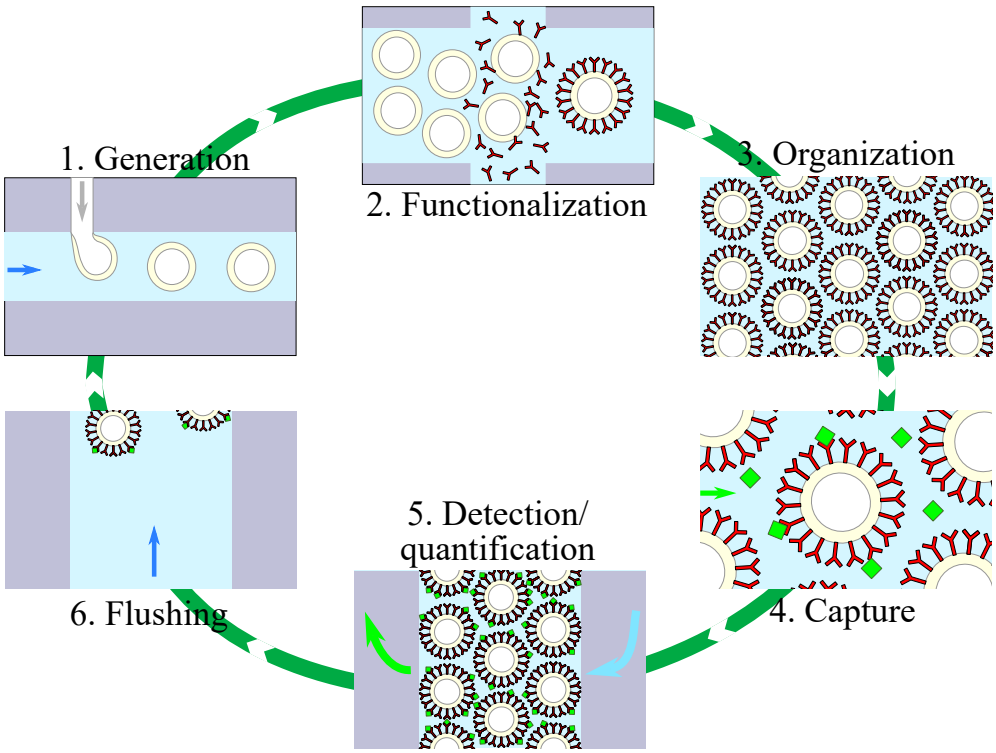

Fig. 1 Principle of operation of a micro-bubbles based regenerable microfluidic biosensor.

2 Functionalization of microbubbles

The first important aspect in the development of the sensor is the step of functionalization of the MBs. We highlight in this section a new fast procedure for decorating the surface of MBs with a ligand taking advantage of the microbubbles generation in a microfluidic chip.

2.1 Microfluidic chip and setup

A specific microfluidic architecture is designed in order to generate, functionalize, and organize the MBs as well as capture an analyte at their surface within the microfluidic chip. The chip (Fig. 2) is composed of 4 inputs (I1 to I4) and one output (O1). I1 and I2 are meeting in a T-Junction and are respectively used for the continuous phase (water based solution) and the disperse phase (gas) used in the functionalized MBs generation process. I3 is used to bring the bioanalyte solution to the chamber where the generated MBs are organized. I4 is used to slowly rinse with an aqueous solution. The I3 and I4 branching inputs uses five-level binary-tree shaped channels of 20µm width in order to have a uniform distribution of bioanalyte solution and rinsing solutions in the broad chamber (Azzopardi et al. (2017)). The square chamber has a side of 3,6 mm while the T-Junction has a width of 100 µm and 20 µm for the continuous and disperse phase respectively. All the channels and the chamber have the same depth of 50 µm.

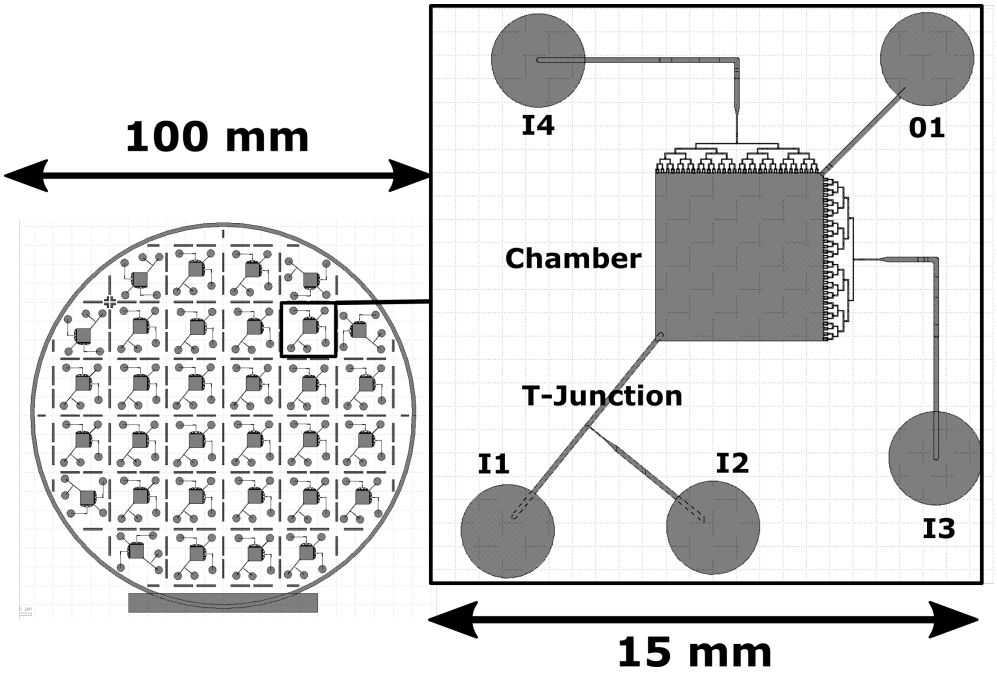

Fig. 2 Layout of wafer with multiple chips and detailed view of one chip for bioanalyte capture.

The microfluidic chips are fabricated using standard soft lithography process (Fig.3), allowing to easily produce PDMS/glass chips.

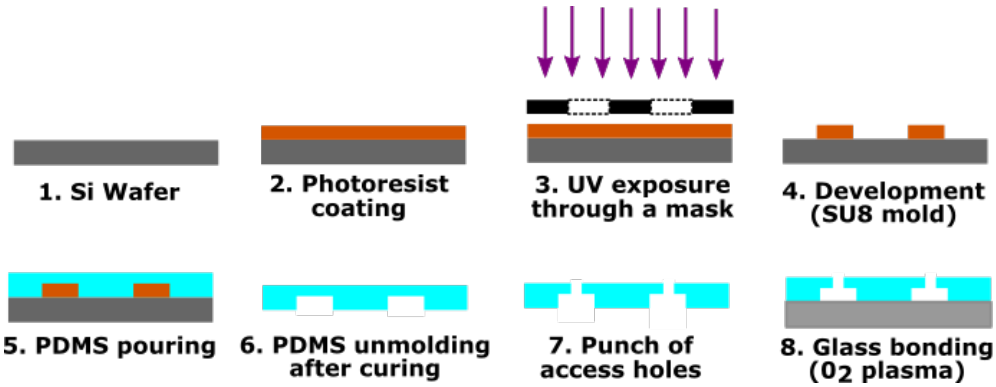

Fig. 3 PDMS/glass chip microfabrication process flowchart.

We base our fabrication on 100 mm wafers, fabricating 32 chips (15x15 mm) per wafer (Fig. 2). A SU8 mold is first patterned in a clean room using thick photoresist. The photoresist (SU8 3050, Kayaku) is spin-coated on the silicon wafer to a thickness of 50 µm. The thickness of the photoresist layer is primordial as it determines the depth of the channels which in turn impacts the minimum size of the bubbles. We cure the photoresist at 95°C using a temperature ramp and waiting overnight for relieving stress to avoid surface cracks and loss of adhesion. Then we expose the photoresist through a photolithography mask at a dose of 200mJ/cm^2 in the mask aligner (EVG 620NT, EVG Group). This chemically amplified photoresist needs a post exposure bake at 95°C before developing in the SU8 developer, rinsing with ethanol and drying with dry nitrogen. A final hard bake for 30 min at 150°C ends the mold-making process. PDMS is prepared by mixing monomer with hardener in a 10:1 ratio by weight and degassing for 30 min in a small vacuum chamber. We then pour a fixed volume of PDMS over the mold and cure it at 80°C in an oven for 4 h. Small parts of the cured PDMS corresponding to one single microfluidic chip are cut and peeled carefully from the mold, before access holes are punched at a diameter of 1.25 mm using a biopsy punch, slightly smaller than the 1/16" OD tubes used in our experiments. The chip is finally closed by bonding glass (BF33) to the PDMS after surface preparation with an O_2 plasma at 100W during 1 min in a dedicated chamber (Plasma Cute, Femto Science).

The test setup (Fig. 4) uses a standard T-Junction configuration (Tarchichi et al. (2013)) with two pressure controllers (Mitos P-Pump, Dolomite microfluidics), one connected to a vial with an aqueous solution and a flow sensor (mini CORI-FLOW, Bronkhorst) for the continuous phase and the other one with direct connection for the disperse phase. For injecting both the analyte and the rinsing solutions, we control the pressure manually with a high resolution manometer directly connected to the internal compressed air network (up to 10 bars). The manometer is connected to two

50 mL Falcon vials hermetically sealed (P-Cap, Fluigent), one being filled with the analyte solution, the other one with an aqueous solution for rinsing. Two pressure sensors are also placed after the vials for monitoring the input pressures. Each input and the output have on-off valves placed just before the chip port for controlling the different steps of operation of the microfluidic chip. Moreover, all inputs have their own cleaning loop using T-valves for facilitating the expulsion of residues out of the chips when necessary. These cleaning loops are not shown in the figure to make the schematic simpler to understand. The output of the chip is linked directly to a beaker to recuperate the produced foam. We developed an instrumentation system using Python (Muller (2022)) to precisely control the pressure controllers and sensors to obtain repeatable flow rate and pressures. For observation of the microbubbles in the chamber we can place the setup under a long working distance microscope (Mitutoyo) equipped with a visible light camera (Flea3, Flir) or under a fluorescence microscope (Axio with Apotome, Zeiss) for fluorescence observation.

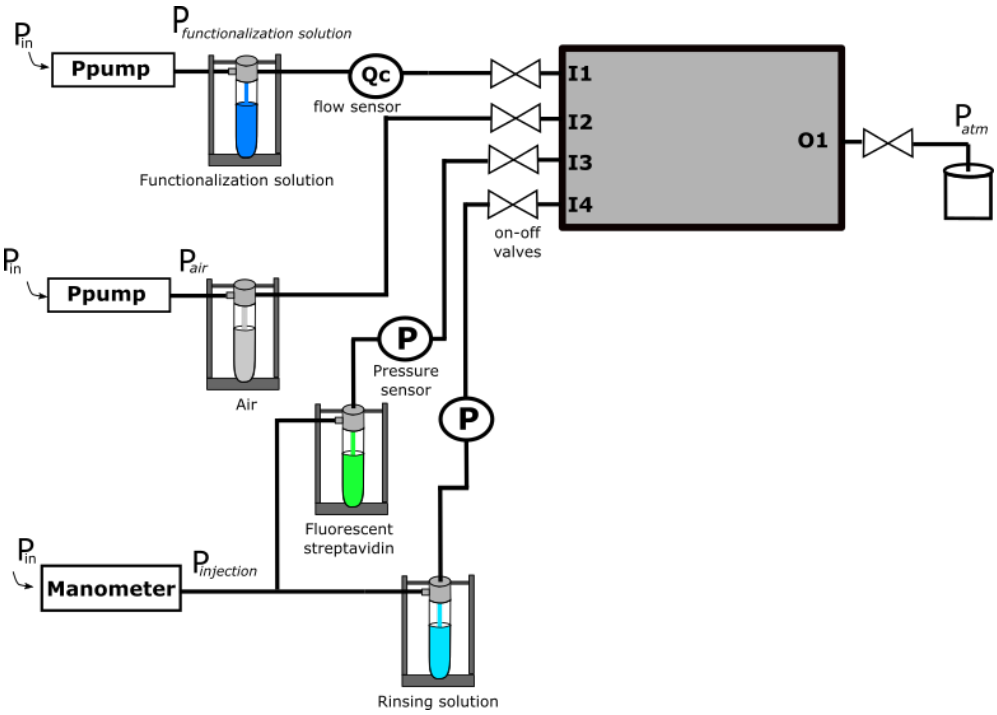

Fig. 4 Setup for control and observation of capture of analyte at the surface of functionalized microbubbles.

2.2 Generation of functionalized microbubbles

For the production of the microbubbles, we decided to combine directly the steps of generation and functionalization, so that the microbubbles are directly decorated with

ligand at the T-junction during their formation, avoiding more complicated microfluidic structures for that specific step. To capture streptavidin, our test bioanalyte, we need to functionalize the surface of the microbubbles with biotin. We note that the biotin functionalization opens up further opportunities for more complex affinity test targeting a broad range of bioanalyte of interest.

To reach that goal, the continuous phase contains at the same time the surfactants for the stability of the bubbles, as well as the lipids for its functionalization. We use phosphatidylethanolamine (PE), a common zwitterionic phospholipid with an amphiphilic character (Petelska et al. (2012)), that place itself at the air/liquid interface. Two PE based functionalization solution were developed: PE CF and DSPE-PEG-Biotin, as shown in Tab. 1.

ID	Composition	Concentration	Usage
FS1	PE CF and SDS in PBS 1 X	10% PE CF at 1 mg/ml and 90% SDS at 1.5%	Observation
FS2	DSPE-PEG-Biotin and SDS in PBS 1 X	10% DSPE-PEG-Biotin at 10mg/ml and 90% SDS at 1.5%	Biotin decoration

Table 1 Solutions for fluorescence observation and biotin decoration of microbubbles

The first solution (FS1) is used for functionalization observation in a stable foam. In fact, PE CF (green fluorescent tagged phosphatidylethanolamine at 1 mg/ml in chloroform, Avanti Polar Lipids) is fluorescent (emission maximum at 515 nm) allowing to easily check the bubbles functionalization with a fluorescent microscope. The second solution (FS2) is used for foam stabilization and the capture of streptavidin, and we used a polymer conjugated phospholipid (DSPE-PEG(2000) with biotin (biotin conjugated polyethylene glycol-2000 at 10mg/ml in chloroform, Avanti Polar Lipids). The lipid solutions are prepared with DMSO as this polar solvent facilitates the lipid dissolution in the PBS 1X and helps the lipid migration to the air/liquid interface, as we previously proposed in Pinon et al. (2018) for the migration of lipids at oil/water interface. The original chloroform solvent is first evaporated and 10 mL DMSO (Sigma Aldrich) is added to obtain the concentrated phospholipid solutions. Regarding the surfactant solution, we mainly used SDS in PBS 1X, but Tween20 in PBS was also used at the beginning without noticeable changes in the experiments. The concentration of surfactant must be optimized, as it needs to be above the Critical Micelle Concentration (CMC) in order to have enough stability of the foam, while having a minimum amount of micelles inside the solution to avoid the perturbation of the migration of the lipids at the interface, as we observed previously with oil droplets (Pinon et al. (2018)). Therefore, we studied the stability of microbubbles produced with different concentrations of SDS to find the minimum concentration yielding a stable foam. For SDS in PBS 1x we found a typical concentration of 1.5% about 10 times above the CMC of 4.61±0.01 mM (Fuguet et al. (2005)). The phospholipid solutions are then mixed (10%) with the surfactant solution (90%), to obtain the two functionalization solutions.

We first generated bubbles using FS1 as the continuous phase to study the presence of a lipidic shell at bubbles surface. By controlling the flowrate and pressure of the continuous and disperse phase, we generate microbubbles at the T-Junction in a jetting generation mode (Tarchichi et al. (2013)). The microbubbles fills the chamber in a few seconds and are monodisperse. For example, the optical view and the corresponding histogram in (Fig. 5-top and left) revels MBs with a diameter standard deviation $\sigma = 3.58$µm for an average diameter $\bar{d} = 100.6$ µm, that is, a polydispersity index of $\psi = \sigma/\bar{d} = 3.5\%$ meeting the criterium for monodispersity ($\psi < 10\%$). Their size is determined by the flow rate of the continuous phase, the pressure of the gas phase and by the size of the channels. More precisely, the larger the continuous phase flow rate, the smaller is the bubble size (Fig. 5-right), with a minimum determined by the depth of the channel. The gas pressure has a smaller influence on MBs size, inducing, for example, a maximum increase of less than 25% of the diameter when the pressure goes from 100 mbar to 500 mbar as the continuous phase flow rate is kept constant at 150 µL/min. We may note that as soon as the MBs diameter exceeds the channel depth (here 50 µm), the bubbles generated are no more spherical but are more like barrels with flattened top and bottom at the floor and ceiling of the channel/chamber. Some combinations of pressure and flow rate do not allow to generate MBs at all or give unstable generation. However, by varying pressure and flow rate in a wide range using the high precision pressure controller of the experimental set-up, we were able to generate repeatably monodisperse MBs with diameter varying between about 50 µm and 400 µm (albeit, with less stability of the generation with the larger MBs).

As the PE CF is fluorescent, we can directly assess the presence of a lipidic shell at the MBs surface with a fluorescent microscope. We first measured the fluorescent emission of all the liquids used to verify that the fluorescence comes only from the lipid and the streptavidin solutions to validate respectively the functionalization and later the capture at bubbles surface. A sample (200 µl) of each liquid used to prepare the functionalization solutions is read by a fluorescent spectrometer with an excitation around 484 nm, and the measured fluorescence spectra are shown in Fig. 6. It appears that only the functionalization solution that contains PE CF and the fluorescent streptavidin solution have a distinct emission, so that the auto-fluorescence of the others liquids can be neglected.

To avoid any artefacts that could be linked with the microfluidic chip itself, we collected with a pipette the foam produced with FS1 at the chip output and placed the MBs between microscope slide and cover-slip. The images obtained with the fluorescence microscope (Fig. 7) showed a clear fluorescent halo around the bubbles, confirming the presence of the lipidic shell. Note that the diameter of the bubbles is here larger (several hundreds of microns) than in the microfluidic chamber as they are not confined anymore in a microchannel and are at atmospheric pressure.

The high speed of functionalization of the MBs in our chip brings a clear advantage over standard MBs and solid surface functionalization procedures. In fact in these cases, functionalization requires several tens of minutes to hours of preparation to ensure a good coverage of the targeted surface with biotin.

The standard functionalization protocols of MBs for targeted imaging or therapy applications (Cho et al. (2006); Takalkar et al. (2004); Yeh et al. (2015); Wang et al.

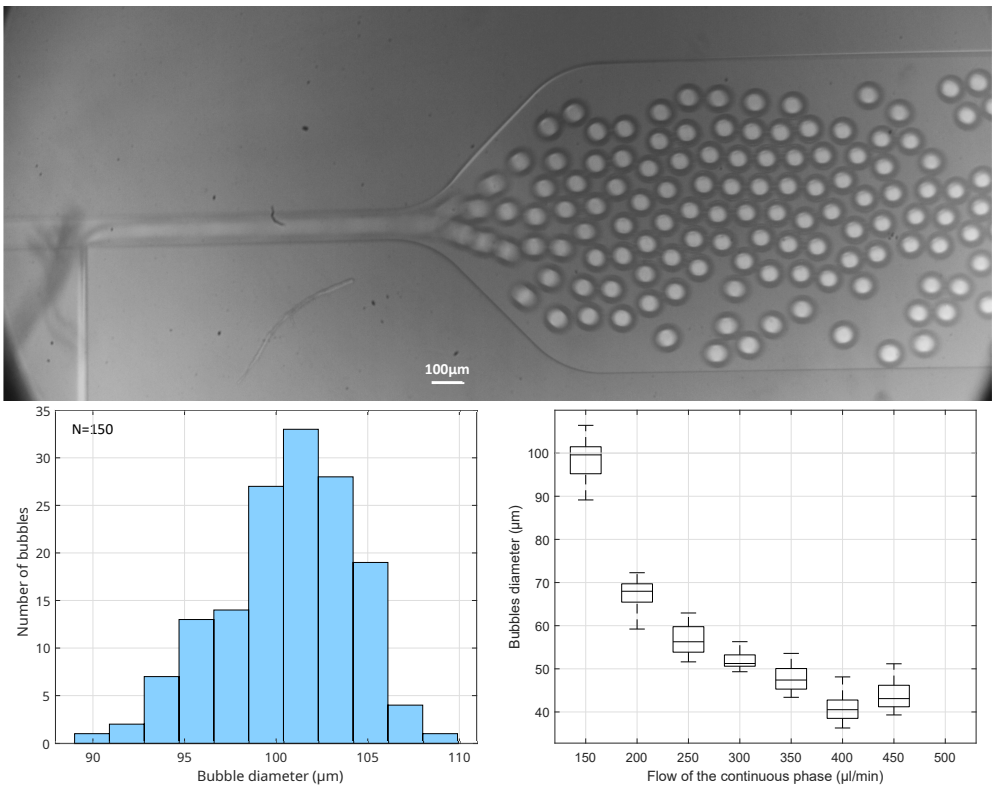

Fig. 5 Generation of microbubbles: (Top) Generation of microbubbles (continuous phase flow rate 150 µl/min and disperse phase pressure 550 mbar). (Bottom) Left: Histogram of the diameter of the generated bubbles showing a polydispersity index of 3.5%. Right: Typical influence of the continuous flow rate on bubble diameter with disperse phase pressure 550 mbar (statistics obtained with N=20, explaining for the flowrate 150µL/min the slight differences in mean with the histogram obtained with N=150).

(2018)) are not frequently detailed in the literature. Still, they often follow a protocol using also a mixture of polymer conjugated phospholipid, however the MBs generation is not performed with microfluidics but is generally based on gas sonication. The resulting bulk production of decorated MBs requires then several centrifugation-flotation steps for rinsing, making their production time consuming and complex for further use as sensing surface in a microfluidic chip. The solid surface functionalization used for biosensing in microchips is generally conducted on oxyde ($SiO-2$, TiO_2, ...) or gold surfaces (Oseev et al. (2021); Focsan et al. (2016)). On oxides, the wet protocol involves a step of hydroxylation of the surface to obtain -OH radicals that will react with APTES silane to finally obtain amine terminated chains at the surface. These two steps takes normally more than 1 hour, although many reports describes duration much larger (6h, over night, etc), they turn out to be based mostly on conviction rather than experimental proof (Sypabekova et al. (2022)). Vapour phase silanization cuts on the chemical interaction time, but if we include the time to place samples in

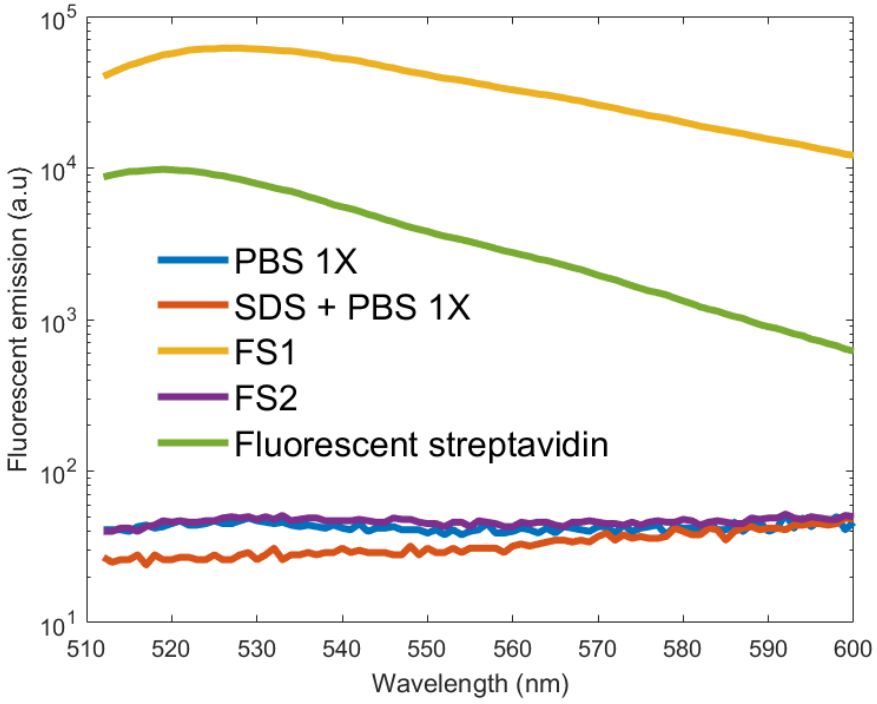

Fig. 6 Fluorescent emission of the different solutions (excitation wavelength around 484 nm).

a vacuum chamber it still exceed several tens of minutes of process. A similar protocol has been developed for gold surface amine functionalization and it replaces the hydroxylation step with a thiol based incubation step that leaves carboxyl group at the metal surface. A further immersion in EDC/NHS solution will results in amine terminated surfaces. Again these two steps take hours to perform (Oseev et al. (2021)). Finally, on oxide or gold surfaces, the bioreceptor of interest need to be grafted over the amine terminated functionalization. In our case the chosen bioreceptor is biotin and biotinylation of the amine surface will require a few more hours (using for example NHS-Biotin) to ensure a good coverage with the right orientation of the biotin (Ye et al. (2007)) on the surface.

The paradigm is significantly different with the microfluidics based surface functionalization of MBs we propose. The amphiphilic nature of the PE phospholipid will help place it at the air/liquid interface, bringing directly the carried biotin functionalization with the right orientation at the MBs surface. The transport of the relatively small functionalization molecules by diffusion is very fast in the microscale channels and it is completed during and after generation, before the MB reaches the chamber in a fraction of second. In a nutshell, we can say that if solid surface functionalization requires transport of the species to the surface followed by chimisorption, our protocol of functionalization of MBs requires only transport, resulting in a much faster process.

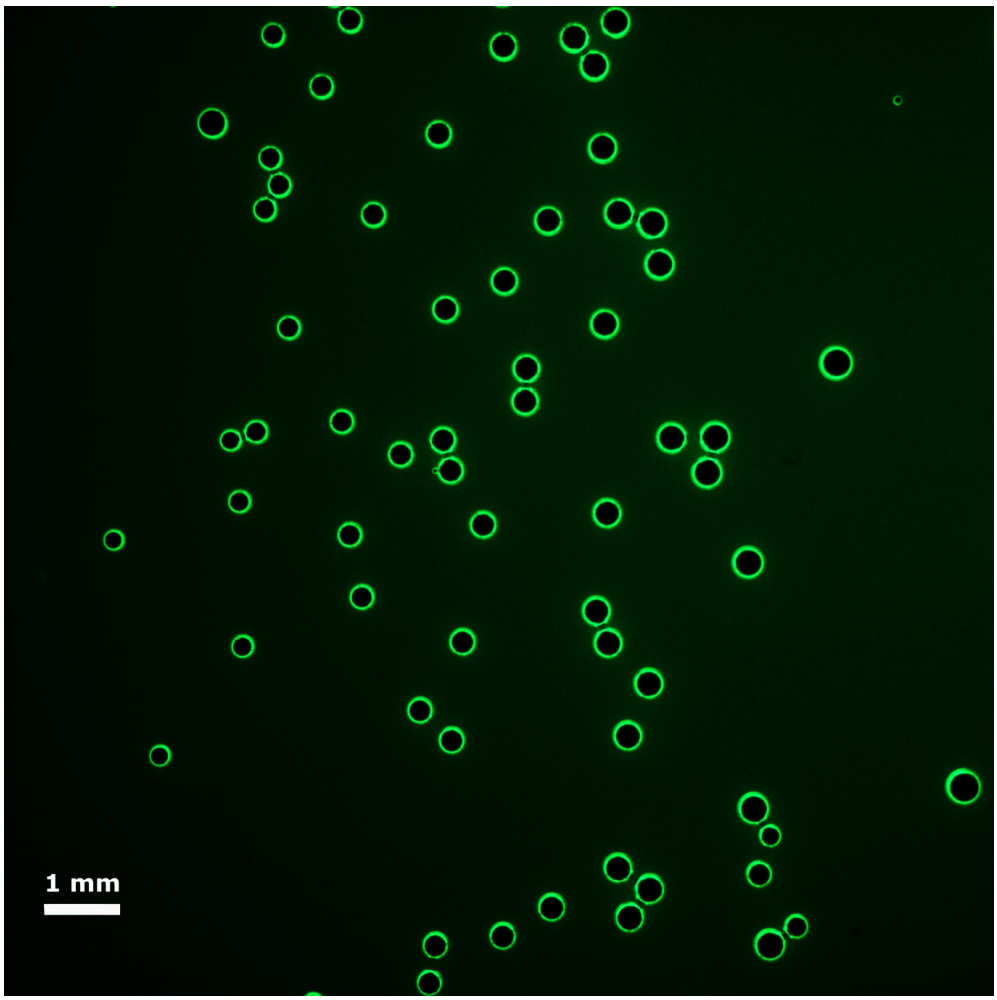

Fig. 7 Functionalized microbubbles with FS1 observed outside the chip with fluorescent microscopy (excitation at 484 nm) (image has been contrast enhanced for edition).

To demonstrate that the biotinylated phospholipids at the surface of the bubbles may act as active ligand we will now present the capture of an analyte within the microfluidic chip.

3 Capture of bioanalytes at bubbles surfaces

3.1 Static organisation of the biotinylated microbubbles

Streptavidin will be the test analyte that will readily interact with the biotinylated MBs surface. Still to increase the chance of interaction we will flow the analyte solution through a static network of MBs inside a chamber. This whole process can be

obtained by controlling the on-off valves of the biochip following the overall sequence summarized in Tab. 2.

Steps	I1	I2	I3	I4	O1	Duration
Generation & Functionalization	O	O	X	X	O	3 sec
Organisation	O	O	X	X	X	1 min
Infusion	O	O	O	X	X	2 min
Rinse	O	O	X	O	X	2 min
Observation	O	O	X	X	X	1 min
Flush & Regeneration	O	O	X	X	O	3-sec

Table 2 Position of on/off valves for the operation of the biosensor (O: on/off valve is open, X: on/off valve is closed) and approximate duration of each step of the process.

We first generate the biotinylated microbubbles with FS2 using inputs I1 and I2. The bubbles formation is very fast, around 0.3ms for 87µm diameter MBs, filling the complete chamber in less than 3s. Then, we simply close the on-off valve of the chip (output O1) letting the bubbles organize themselves in a static hexagonal network.(Fig. 8).

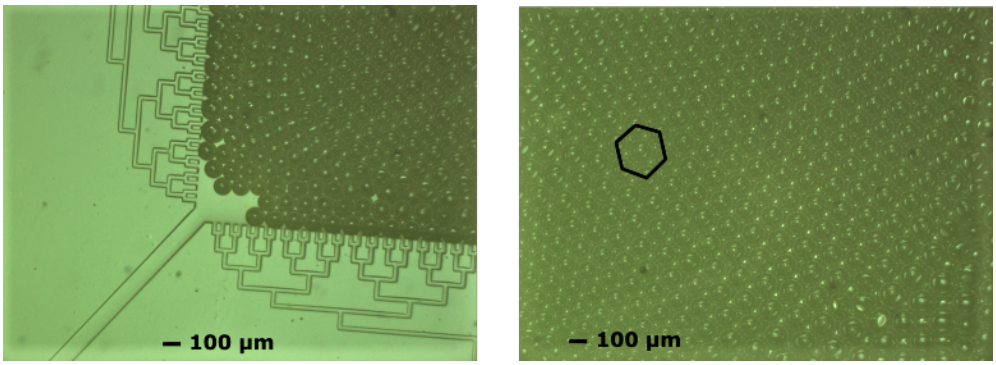

Fig. 8 Static organization of the microbubbles inside the chamber, forming a static hexagonal network. (image has been contrast enhanced for edition)

We observed a good stability of the MBs network in the microfluidic chamber, with a change of diameter of about 13% over the 10 min period necessary to conduct the experiments (Fig. 9), with slight differences of slope according to the initial radius of the bubbles. The aging of the foam is here dominated by ripening, where gas inside the MBs dissolves into the liquid phase. This result is in good agreement with the Epstein-Plesset model (Duncan and Needham (2004)), that describes the evolution of the radius of a free bubble:

$$R(t) = \sqrt{R_0^2 - 2Dk_H N_A k_B T(1-f)t} \tag{1}$$

with R_0 the initial radius, D the diffusion coefficient of the gas within the liquid, $f = \frac{C_0}{C_s}$ the ratio between the concentration of initial gas dissolved in the solution and the concentration at saturation, k_H the Henry constant, N_A the Avogadro's number, k_B the Boltzmann's constant (product $N_A k_b$ is the ideal gas constant) and T the temperature. The equation is solved using the software Maple®, and we notice that the evolution of the radius is particularly sensitive to the value of f. The model shows that the dissolution rate remains constant for a certain time t before increasing, similarly to our experimental values (Fig. 9). Besides, the high sensitivity of this model to the parameter f easily leads to a difference of slopes: according to the initial MBs radius, the air fraction in the chamber differs, and so is the gas saturation of the liquid that could explain the difference of slopes we observe experimentally. Furthermore, we note that the detailed study of the dissolution rate of bubbles, reveals that the proximity of one gas tight wall slows the dissolution of the bubbles with a factor of 1.44 (Duncan and Needham (2004)). It confirms that bubbles inside microfluidic chambers dissolve less quickly than in an "infinite" media, allowing to avoid, in our experiments based on MBs with diameter larger than 80 µm, the injection of low solubility gas such as SF_6, commonly used with contrast enhancing agents (Versluis et al. (2020)).

3.2 Injection and capture of fluorescent streptavidin through the bubbles network

Once the chamber is filled with static microbubbles, the next step is to infuse fluorescent streptavidin through the bubbles network and assess the capture at the surface using fluorescent microscopy. The infusion of the streptavidin solution analyte (Invitrogen Alexa Fluor 488 at 0.01 mg/ml diluted in PBS 1X solution) through the network of bubbles is precisely controlled by pressure to avoid disrupting the bubble array (Fig. 10-a,b). The corresponding on-off valve is opened during 2 min at a low flow rate of about 0.1 µL/min estimated from fluorescent image sequence using Darcy's porous medium flow model with a porosity of 0.2 (Azzopardi et al. (2019)). For observation, we then rinsed the foam for an additional 2 min with a PBS solution in order to remove the fluorescent streptavidin solution between the MBs (Fig. 10-c). We note that a rinsing step may also be inserted before the infusion of the bioanalyte to remove unbound functionalization chemicals, but it wasn't necessary for these initial experiments.

The final observation clearly shows a fluorescent shell around the bubbles (Fig. 10-d) confirming the capture of the streptavidin at the bubbles surface and confirming the possibility to use the presented technique for bioanalyte capture and sensing. We have also conducted an experiment using MBs produced in similar conditions but with a solution without biotin termination on the PE phospholipids. After infusion of fluorescent streptavidin in the MBs array followed a rinsing step with PBS, the MBs did not present a fluorescent shell (Fig. 10-e). This negative-control experiment shows that the streptavidin really binds to the biotin decorating the MB surface and does not exhibit non-specific binding to the MBs air/water interface.

We may compare the capture step in the MBs array and in a traditional biosensor composed of a shallow microfluidic chamber with only its floor decorated with a ligand. A detailed analysis (Squires et al. (2008)) will require considering the Péclet number in the region where the capture happens, but we will reduce it here to the comparaison

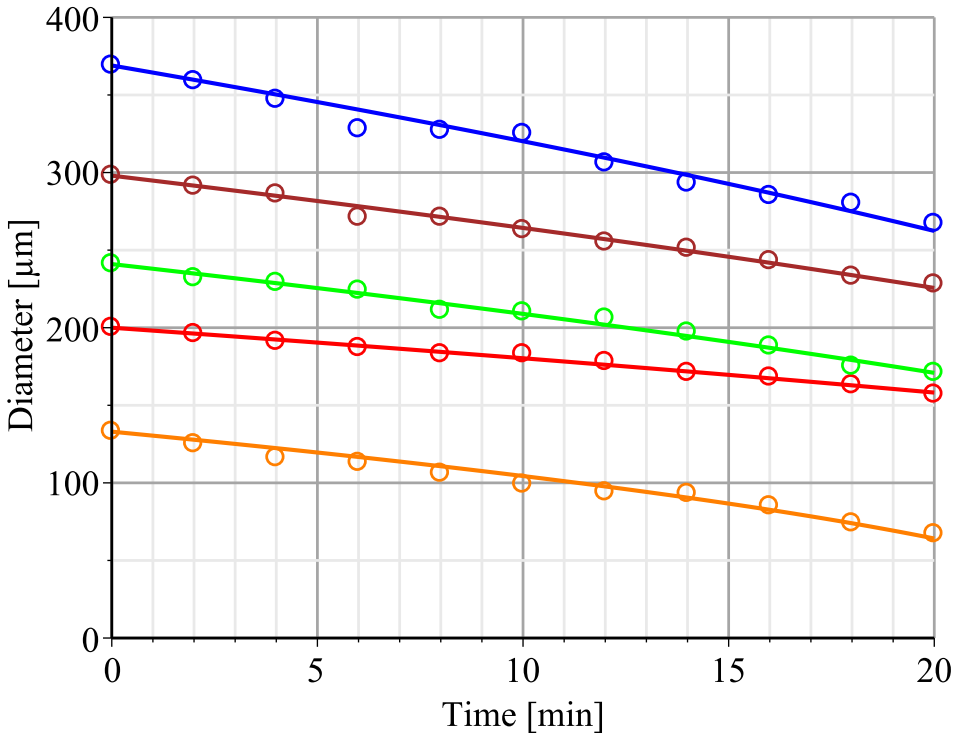

Fig. 9 Experimental evolution of bubble diameter during 20 minutes of static organization for different initial sizes. Lines are least-square fits of the Epstein-Plesset model using f as parameter with Maple®.

of the diffusive flow, and assume all other things are similar. If we assume a chamber 50 µm deep in the classical biosensor, compared to an interval between two MBs of 5 µm during infusion, we see that the ratio of the maximum distance the streptavidin from the test solution needs to travel before it could be captured by biotinylated surfaces is 20. It means that the maximum diffusion time is 400 times shorter in MBs based biosensors than in solid surface biosensors. Although this seems a big factor, it should be noted that in classical biosensors, the transport time for many bioanalyte remains short ($< 1\,\mathrm{s}$) and is orders of magnitude shorter than the functionalization time ($> 1\,\mathrm{h}$) and thus the transport time has little impact on the duration of the complete measurement cycle (as presented in Fig 1) for these biosensors.

Finally, we demonstrated that the ligand decorated MBs array can be fully regenerated by closing both I3 and I4 and then by opening O1 in order to flush the bubbles while a new foam is generated in a few seconds. This speed emphasizes the efficiency of our sensor for functionalized surface regeneration and opens new opportunities, like performing series test for duplicate testing or by using multiple ligands in series, for complex biological analysis. In contrast, solid surface sensors would first require

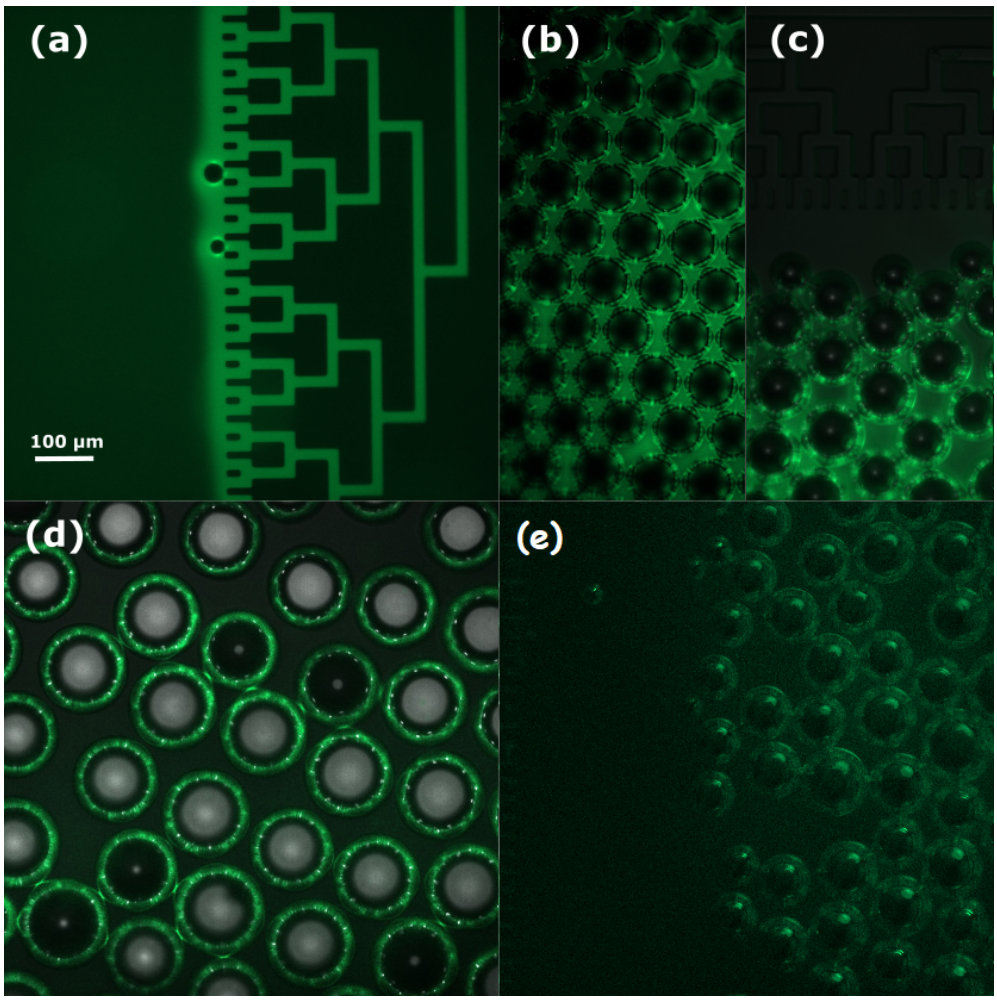

Fig. 10 Capture of fluorescent streptavidin at bubbles surface within the chamber with (a) start of the injection in the chamber (only the input channels are fluorescent) (b) after the streptavidin infusion through the bubbles network is finished (streptavidin is present in the void between bubbles) (c) during rinsing of the free streptavidin (rinsing comes from the top of the image) (d) zoomed view after PBS rinsing showing the streptavidin captured at the bubble surface (e) negative control showing the absence of streptavidin capture at the surface of MBs without biotin decoration

lengthy processes to wash the existing functionalization (Lacour et al. (2016)) and again hour long processes to produce a new ligand decorated surface for performing a new capture. It is no surprise that these type of biosensors have generally to be disposable.

4 Conclusion

In this paper, we demonstrate the possibility to form functionalized MBs directly during their generation in a microfluidic chip. While functionalized MBs provide outstanding results in medical imagery and therapy, this work aims at using microbubbles surface as a biointerface in order to make a fast regenerable biosensor. Therefore, a microfluidic architecture adapted for this application is presented, that produces biotinylated MBs using a T-Junction and organizes them statically in a chamber. We manage to inject a solution of fluorescent streptavidin through the network of MBs while maintaining its static organization. After rinsing, the capture of the streptavidin is made evident by fluorescence. In the future, we plan to base the quantification on a label-free approach, using the change in acoustic resonance of MBs after analyte capture. The regeneration of the sensor is simply done by flushing the bubbles out of the chip and producing a new MBs array. The complete operation sequence - including ligand functionalization, capture, measurement and sensor regeneration - takes less than ten minutes, much faster than for the current biosensors based on solid surface functionalization (such as lateral flow test or QCM based acoustic biosensors).

Acknowledgments. This work was supported by the french RENATECH network and its FEMTO-ST technological facility. We acknowledge the support of the CNRS/Univ. Bourgogne Franche-Comté CLIPP platform for biochemistry work and analysis. This work has been supported by the EIPHI Graduate school (contract "ANR-17-EURE-0002") and by the Bourgogne-Franche-Comté Region. A special thanks goes to Tristan Muller for the help on the instrumentation of the setup, to Laurent Robert for the clean room part of the fabrication and to Alain Rouleau for his help regarding chemistry work.

Declaration

- Competing interests
  The authors have no competing interests as defined by Springer, or other interests that might be perceived to influence the results and/or discussion reported in this paper.
- Data Availability
  The data that support the findings of this study are available from the corresponding author upon reasonable request.

References

Azzopardi, C.-L., Chollet, F., Manceau, J.-F., Boireau, W.: Analyte capture in an array of functionalized droplets for a regenerable biosensor. Biomicrofluidics **13**(5), 054105 (2019) https://doi.org/10.1063/1.5115494

Azzopardi, C.-L., Lacour, V., Manceau, J.-F., Barthès, M., Bonnet, D., Chollet, F., Leblois, T.: A fluidic interface with high flow uniformity for reusable large area resonant biosensors. Micromachines **8**(10), 308 (2017) https://doi.org/10.3390/mi8100308

Beguin, E., Bau, L., Shrivastava, S., Stride, E.: Comparing strategies for magnetic functionalization of microbubbles. ACS Applied Materials & Interfaces **11**(2), 1829–1840 (2019) https://doi.org/10.1021/acsami.8b18418

Chowdhury, S.M., Abou-Elkacem, L., Lee, T., Dahl, J., Lutz, A.M.: Ultrasound and microbubble mediated therapeutic delivery: Underlying mechanisms and future outlook. Journal of Controlled Release **326**, 75–90 (2020) https://doi.org/10.1016/j.jconrel.2020.06.008

Cho, S.H., Jeong, J.H., Yang, S.R., Kim, B.Y., Kim, J.-D.: Binding evaluation of targeted microbubbles with biotin–avidin interaction by surface plasmon resonance biosensor. Japanese journal of applied physics **45**(1S), 421 (2006) https://doi.org/10.1143/jjap.45.421

Dundas, C.M., Demonte, D., Park, S.: Streptavidin–biotin technology: improvements and innovations in chemical and biological applications. Applied microbiology and biotechnology **97**, 9343–9353 (2013) https://doi.org/10.1007/s00253-013-5232-z

Duncan, P.B., Needham, D.: Test of the epstein- plesset model for gas microparticle dissolution in aqueous media: effect of surface tension and gas undersaturation in solution. Langmuir **20**(7), 2567–2578 (2004) https://doi.org/10.1021/la034930i

Focsan, M., Campu, A., Craciun, A.-M., Potara, M., Leordean, C., Maniu, D., Astilean, S.: A simple and efficient design to improve the detection of biotin-streptavidin interaction with plasmonic nanobiosensors. Biosensors and Bioelectronics **86**, 728–735 (2016) https://doi.org/10.1016/j.bios.2016.07.054

Fuguet, E., Ràfols, C., Rosés, M., Bosch, E.: Critical micelle concentration of surfactants in aqueous buffered and unbuffered systems. Analytica Chimica Acta **548**(1-2), 95–100 (2005) https://doi.org/10.1016/j.aca.2005.05.069

Gramiak, R., Shah, P.M.: Echocardiography of the aortic root. Investigative radiology **3**(5), 356–366 (1968) https://doi.org/10.1097/00004424-196809000-00011

Kogan, P., Gessner, R.C., Dayton, P.A.: Microbubbles in imaging: applications beyond ultrasound. Bubble Science, Engineering & Technology **2**(1), 3–8 (2010) https://doi.org/10.1179/175889610X12730566149100

Lacour, V., Elie-Caille, C., Leblois, T., Dubowski, J.J.: Regeneration of a thiolated and antibody functionalized gaas (001) surface using wet chemical processes. Biointerphases **11**(1) (2016) https://doi.org/10.1116/1.4942878

Langeveld, S.A.G., Meijlink, B., Kooiman, K.: Phospholipid-coated targeted microbubbles for ultrasound molecular imaging and therapy. Current Opinion in Chemical Biology **63**, 171–179 (2021) https://doi.org/10.1016/j.cbpa.2021.04.013

Muller, T.: BiAcoustic PID Flowrate. GitLab (2022). https://gitlab.com/mllr.tristan/

projetm2

Oseev, A., Lecompte, T., Remy-Martin, F., Mourey, G., Chollet, F., Boiseau-marie, B.L.R., Rouleau, A., Bourgeois, O., Maistre, E., Elie-Caille, C., Manceau, J.-F., Boireau, W., Leblois, T.: Assessment of shear-dependent kinetics of primary haemostasis with a microfluidic acoustic biosensor. IEEE Transactions on Biomedical Engineering **68**(8), 2329–2338 (2021) https://doi.org/10.1109/tbme.2020.3031542

Pinon, L., Montel, L., Mesdjian, O., Bernard, M., Michel, A., Ménager, C., Fattaccioli, J.: Kinetically enhanced fabrication of homogeneous biomimetic and functional emulsion droplets. Langmuir **34**(50), 15319–15326 (2018) https://doi.org/10.1021/acs.langmuir.8b02721

Petelska, A.D., Naumowicz, M., Figaszewski, Z.A.: The influence of ph on phosphatidylethanolamine monolayer at the air/aqueous solution interface. Cell Biochemistry and Biophysics **65**(2), 229–235 (2012) https://doi.org/10.1007/s12013-012-9424-4

Sypabekova, M., Hagemann, A., Rho, D., Kim, S.: Review: 3-aminopropyltriethoxysilane (aptes) deposition methods on oxide surfaces in solution and vapor phases for biosensing applications. Biosensors **13**(1), 36 (2022) https://doi.org/10.3390/bios13010036

Squires, T.M., Messinger, R.J., Manalis, S.R.: Making it stick: convection, reaction and diffusion in surface-based biosensors. Nature Biotechnology **26**(4), 417–426 (2008) https://doi.org/10.1038/nbt1388

Tarchichi, N., Chollet, F., Manceau, J.-F.: New regime of droplet generation in a T-shape microfluidic junction. Microfluidics and Nanofluidics **14**, 45–51 (2013) https://doi.org/10.1007/s10404-012-1021-8

Takalkar, A.M., Klibanov, A.L., Rychak, J.J., Lindner, J.R., Ley, K.: Binding and detachment dynamics of microbubbles targeted to p-selectin under controlled shear flow. Journal of Controlled Release **96**(3), 473–482 (2004) https://doi.org/10.1016/j.jconrel.2004.03.002

Unger, E.C., Matsunaga, T.O., McCreery, T., Schumann, P., Sweitzer, R., Quigley, R.: Therapeutic applications of microbubbles. European Journal of Radiology, 160–168 (2002) https://doi.org/10.1016/s0720-048x(01)00455-7

Unger, E., Porter, T., Lindner, J., Grayburn, P.: Cardiovascular drug delivery with ultrasound and microbubbles. Advanced Drug Delivery Reviews **72**, 110–126 (2014) https://doi.org/10.1016/j.addr.2014.01.012

Versluis, M., Stride, E., Lajoinie, G., Dollet, B., Segers, T.: Ultrasound contrast agent modeling: A review. Ultrasound in Medicine & Biology **46**(9), 2117–2144 (2020)

https://doi.org/10.1016/j.ultrasmedbio.2020.04.014

Wang, S., Hossack, J.A., Klibanov, A.L.: Targeting of microbubbles: contrast agents for ultrasound molecular imaging. Journal of Drug Targeting **26**(5–6), 420–434 (2018) https://doi.org/10.1080/1061186x.2017.1419362

Warram, J.M., Sorace, A.G., Saini, R., Umphrey, H.R., Zinn, K.R., Hoyt, K.: A triple-targeted ultrasound contrast agent provides improved localization to tumor vasculature. Journal of Ultrasound in Medicine **30**(7), 921–931 (2011) https://doi.org/10.7863/jum.2011.30.7.921

Yang, J., Miao, X., Guan, Y., Chen, C., Chen, S., Zhang, X., Xiao, X., Zhang, Z., Xia, Z., Yin, T., Hei, Z., Yao, W.: Microbubble functionalization with platelet membrane enables targeting and early detection of sepsis-induced acute kidney injury. Advanced Healthcare Materials **10**(23), 2101628 (2021) https://doi.org/10.1002/adhm.202101628

Ye, L., Pelton, R., Brook, M.A.: Biotinylation of tio2 nanoparticles and their conjugation with streptavidin. Langmuir **23**(10), 5630–5637 (2007) https://doi.org/10.1021/la0626656

Yeh, J.S.-M., Sennoga, C.A., McConnell, E., Eckersley, R., Tang, M.-X., Nourshargh, S., Seddon, J.M., Haskard, D.O., Nihoyannopoulos, P.: A targeting microbubble for ultrasound molecular imaging. PLOS ONE **10**(7), 0129681 (2015) https://doi.org/10.1371/journal.pone.0129681